Understanding Antiferromagnetic and Ligand Field Effects on Spin Crossover in a Triple-decker Dimeric Cr(II) Complex

Arup Sarkar,[1] Matthew R. Hermes,[1] Christopher J. Cramer[2], John S. Anderson[1] and Laura Gagliardi[3,*]

[1]*Department of Chemistry, The University of Chicago, Chicago, IL-60637 USA*
[2]*UL Research Institutes, 333 Pfingsten Road, Northbrook, IL 60062 USA.*
[3]*Department of Chemistry, Pritzker School of Molecular Engineering, James Franck Institute, Director of the Chicago Center for Theoretical Chemistry, The University of Chicago, Chicago, IL-60637 USA*
KEYWORDS. Spin Crossover, Multireference methods, Antiferromagnetic coupling, Ligand-field.

ABSTRACT: Two possible explanations for the temperature-dependence of spin crossover (SCO) behavior in the dimeric triple-decker Cr(II) complex ([(η^5-C_5Me_5)Cr(μ^2:η^5-P^5)Cr(η^5-C_5Me_5)]$^+$) have been offered. One invokes variations in antiferromagnetic interactions between the two Cr(II) ions, while the other posits the development of a strong ligand-field effect favoring the low-spin ground state. We perform multireference electronic structure calculations based on multiconfiguration pair-density functional theory to resolve these effects. We find quintet, triplet, and singlet electronic ground states, respectively, for the experimental geometries at high, intermediate, and low temperatures. The ground-state transition from quintet to triplet at intermediate temperature derives from increased antiferromagnetic interactions between the two Cr(II) ions. By contrast, the ground-state transition from triplet to singlet at low temperature is attributable to increased ligand-field effects, which dominate with continued variations in antiferromagnetic coupling. This study provides quantitative detail for the degree to which these two effects can act in concert for the observed SCO behavior in this complex and others subject to temperature dependent variations in geometry.

1. Introduction

Spin-crossover (SCO) complexes exhibit cooperative spin transitions[1,2,3,4,5] with changes in temperature, pressure, light, or other external stimuli. [6,7,8,9] These transitions can lead to thermal hysteresis, which has enabled the development of SCO-based applications such as memory storage, spin switching, molecular electronics, and molecular sensors.[2,10,11,12] In these systems, transition metal (TM) ions typically change from a high spin (HS) state at higher temperatures to a low spin (LS) state at lower temperatures, accompanied by a reduction in metal-ligand bond length. SCO is a collective property that affects many molecules within a sample over a wide temperature range, and sharper transitions are typically due to cooperative structural changes in the solid-state. The equilibrium populations of high spin (HS) and low spin (LS) state within a sample are equal at the transition temperature, or $T_{1/2}$, for a spin-crossover (SCO) complex. The most extensively studied SCO complexes have been six-coordinate Fe(II) species, which undergo spin-state changes from S = 2 (HS) to S = 0 (LS) via a one-step mechanism or sometimes through an intermediate S = 1 state via a two-step mechanism.[13 ,14,15,16,17] Other transition metal ions, such as Fe(III), Cr(II), Mn(III), and Co(II), are also known to exhibit SCO behavior.[18,19,20,21] However, their properties and potential applications are not, in general, as well understood as those of Fe(II)-based complexes.

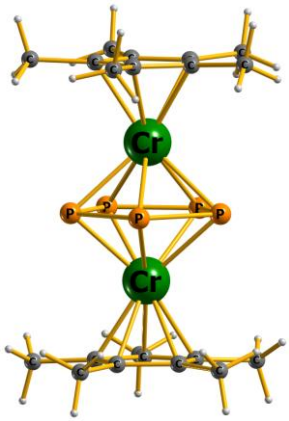

Figure **1**. [(η^5-C_5Me_5)Cr^{II}(μ^2:η^5-P^5)Cr^{II}(η^5-C_5Me_5)]$^+$ complex. Color code- green: Cr, orange: P, deep grey: C and light grey: H.

TM complexes with two or more open-shell metal ions connected via a bridging ligand can exhibit strong electron correlation due to the overlap of magnetic orbitals and associated magnetic interactions (ferro or anti-ferro) between the spin centers, particularly with short 1-2 atom bridges.[22,23,24] In 1994, Hughes et al. studied the variable temperature

magnetic susceptibility of a dimeric triple-decker Cr(II) complex $[(\eta^5\text{-}C_5Me_5)Cr(\mu^2{:}\eta^5\text{-}P^5)Cr(\eta^5\text{-}C_5Me_5)]^+$ (henceforth "the dimer;" Figure **1**) and reported that the dimer behaves as two isolated S = 1 systems at high temperature (160 K-295 K).[25] In a subsequent study in 2007, Goeta et al. reported molecular structures of the dimer obtained by X-ray diffractometry (XRD) at sixteen different temperatures spanning the spin crossover region indicated from magnetic susceptibility experiments (i.e., the χT vs. T curve).[26] Interestingly, the XRD experiments showed two different, independent dimeric units coexisting in the unit cell over the temperature range from 12 to 160 K. One unit (cation I) is characterized by an internuclear distance between the two Cr ions that progressively decreases as the temperature is lowered, whereas the other unit (cation II) is characterized by a near-constant Cr–Cr distance as the temperature decreases, followed by an abruptly shorter Cr–Cr distance at 12 K; this behavior is mapped against the experimental magnetic susceptibility curve in Figure **2**. Goeta et al. proposed two possible characterizations of the dimer's electronic structure in light of these experiments:

1. Reduced Cr–Cr internuclear distances increase favorable antiferromagnetic interactions between the Cr ions through, e.g., the formation of Cr–Cr bonding orbitals or through the promotion of super-exchange interactions mediated by the phosphorous ring, or
2. The Cr–Cr internuclear distance is a secondary phenomenon associated with local geometric changes driven by temperature-dependent variations in ligand field effects causing the individual Cr ions to transition from high-spin S = 1 states to low-spin S = 0 states.

These two possibilities cannot be resolved solely from the experimental data. Here, we provide quantitative insight into the relative importance of these effects using the toolkit of computational quantum chemistry.

Density functional theory (DFT) methods are computationally affordable and can, in principle, be used to study the electronic energy states of the SCO complexes.[27,28] Excited state DFT methods such as broken-symmetry DFT and time-dependent DFT are routinely used to rationalize the energy potential and bonding effects within SCO complexes.[29,30] A major complication in single-determinant methods like DFT, however, is that the Kohn-Sham determinant for many open-shell systems is not an eigenfunction of the $\hat{S}^2$ operator. Intermediate spin-state energies in such instances are not necessarily derived from the Kohn-Sham eigenfunction itself, but may instead be computed by reference to a Heisenberg-Dirac-Van Vleck Hamiltonian.[31]

Wavefunction-based methods are typically more computationally costly than DFT but may offer advantages in accuracy. For instance, domain-based pair natural orbital CCSD(T) theory has been found to be superior to DFT-based methods for determining accurate spin state energies in various systems,[32,33] and spin-symmetry adapted multi-reference wave function theories such as CASSCF, CASPT2, and DMRG have also been demonstrated to yield accurate excitation energies.[34,35,36] Recently, Chan and co-workers addressed the benchmark challenge of reproducing the potential energy curve of the Cr_2 molecule using the DMRG-REPT methodology, which is also a multireference quantum chemical technique.[37] While triple-decker systems similar to the above-mentioned dimer involving P_5, P_4, and P_6 bridging ligand systems have been studied previously using DFT methods, multiconfiguration-based approaches have not yet been applied to these systems.[38,39,40,41]

To address the electronic structure of the dimer depicted in Figure **1**, we here employ a combination of complete active space SCF (CASSCF) and restricted active space SCF (RASSCF)[42,43] methods with multi-configuration pair-density functional theory (MC-PDFT)[44,45]. This approach has been shown to compute spin state energy gaps and zero-field splitting with similar accuracies as the more computationally demanding CASPT2 method.[46,47,48,49,50] Our multi-reference calculations revealed that the observed temperature-dependent magnetic susceptibility curve arises from the magnetic moment of two (or more) dimeric cation units, each with different spin states at different temperature ranges. We demonstrated that both antiferromagnetic coupling and ligand field spin transition are responsible for the spin crossover occurring over the temperature range of 150K to 12K. Our results highlight the importance of using multireference electronic structure calculations to accurately predict the correct spin states and mechanisms involved in spin crossover, particularly in cases where there is a metal dimer and single-reference methods may not be accurate enough. Further detail on the theoretical methods is provided in Section **2**. Section **3** describes results from both multireference and DFT theories for single-point calculations of the dimer at the various experimental geometries obtained for different temperatures in Ref 26.[26] Section **3.5**, also quantifies the contributions of antiferromagnetic and strong ligand-field effects on the spin-crossover mechanism, and section **4** provides concluding analysis.

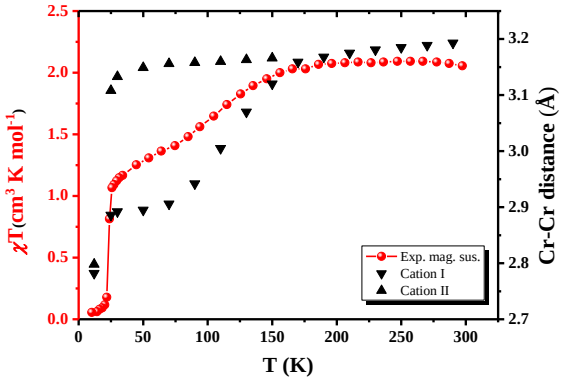

Figure **2**: Experimental χT vs T curve of the dimeric Cr(II) complex (reproduced from Ref. **26**).

2. Theoretical Methods

Vertical spin-state energy gaps for the dimer at the various experimental (XRD) geometries[25,26] were computed using multireference methods (hydrogen positions were not determined from the XRD data, but were instead optimized at the BP86/def2SVP level). To refer to these geometries, we adopt the nomenclature presented in Table **1**. The first subscript refers to the temperature at which the XRD experiment was conducted and, when needed, a Roman numeral is added to distinguish the two distinct dimeric units in the unit cell (cf. Figure **2**).

CASSCF, RASSCF, CASPT2, RASPT2 and MC-PDFT calculations were used to compute spin-state energies. The MC-PDFT calculations used the translated PBE (tPBE) functionals and an ultrafine quadrature grid; these calculations are referred to as CAS-tPBE or RAS-tPBE, depending on the reference wave function (and functional) used. For the CASPT2 and RASPT2 calculations, a default IPEA shift of 0.25 a.u. and an imaginary shift of 0.3 a.u. were used.[51] The resolution-of-the-identity/Cholesky decomposition (RICD) approximation was used to reduce the cost of two-electron integral calculations.[52] Adiabatic geometries and energy gaps for various spin states, with vertical excitation energies reported for the geometry of the quintet optimized at the B3LYP/def2-TZVP level and multireference level have been shown in Sections **S1.1**, **S1.2** and **S1.3** in the supporting information.

Table 1. Shorthand notations used to denote the XRD geometries of the dimer originally reported in Ref. [26] **and referred to in this work.**

Temperature (K)	Labels	
290	X_{290}	
270	X_{270}	
150	$X_{150-\mathrm{I}}$	$X_{150-\mathrm{II}}$
130	$X_{130-\mathrm{I}}$	$X_{130-\mathrm{II}}$
110	$X_{110-\mathrm{I}}$	$X_{110-\mathrm{II}}$
90	$X_{90-\mathrm{I}}$	$X_{90-\mathrm{II}}$
70	$X_{70-\mathrm{I}}$	$X_{70-\mathrm{II}}$
50	$X_{50-\mathrm{I}}$	$X_{50-\mathrm{II}}$
30	$X_{30-\mathrm{I}}$	$X_{30-\mathrm{II}}$
25	$X_{25-\mathrm{I}}$	$X_{25-\mathrm{II}}$
12	$X_{12-\mathrm{I}}$	$X_{12-\mathrm{II}}$

For the multireference calculations, the basis set was def2-TZVP, except for H atoms, for which def2-SVP was used. The RASSCF, RAS-tPBE, and RASPT2 calculations used a (16e,16o) active space consisting of the two Cr(II) 3*d* shells, two occupied orbitals from each of the C_5Me_5 ligands, and two unoccupied orbitals from the bridging P_5 ligand. The latter were found to mix strongly with two Cr 3*d* orbitals indicative of covalent bonding between the Cr atoms and the P_5 ring (cf. Figure **3**). The RAS2 subspace was therefore taken as these two pairs of Cr-P_5-Cr bonding/antibonding orbitals along with four singly occupied Cr 3*d* orbitals, for an overall subspace of (8e,8o). The RAS1 and RAS3 subspaces consisted respectively of the bonding and antibonding π_{xz} and π_{yz} orbitals from the C_5Me_5 ligands and the remaining Cr 3*d* orbitals, with up to two holes in RAS1 and up to two electrons occupying RAS3 (See Section 3 and Figure **3** below). We also performed CASSCF(8e,8o) and corresponding CAS-tPBE and CASPT2 calculations in which the RAS1 and RAS3 subspaces from the above-described (16e,16o) active space were omitted.

Kohn-Sham density functional calculations were performed using ORCA 5.0.0[53] and all multireference calculations were done using *OpenMolcas* version 22.02.[54]

3. Results and Discussion

3.1 *Spin state gaps computed on the X-ray structures*

We computed spin-state energies for the various X-ray structures reported for different temperatures by Goeta *et al*.[26] We examined only the singlet, triplet, and quintet spin states, as preliminary calculations (see Section **S1.2** and **S1.3** of the SI) indicated that the septet and nonet states are very high in energy and do not contribute to the magnetism of the dimer at temperatures below 290 K. We also omitted the XRD geometries at temperatures between 150 K and 270 K, as the magnetic susceptibility does not vary significantly over this temperature range.

Figure **3** presents the optimized RAS(16e,16o) orbitals of the quintet spin state at the X_{290} geometry. (Figures **S3** and **S4** in the SI additionally present the orbitals for the triplet state of $X_{110-\mathrm{I}}$ and the singlet state of $X_{12-\mathrm{I}}$ respectively). The magnetic moment at high temperature clearly derives from the four singly occupied orbitals, two formed from alternative linear combinations of the two metal d_{z^2} orbitals, and the other two being in-phase combinations of the metal d_{xy} and $d_{x^2-y^2}$ orbitals, respectively, with very small contributions from s orbitals of the P_5 ring. The out-of-phase combinations of the metal d_{xy} and $d_{x^2-y^2}$ orbitals (which belong to the E_2 irrep in D_5 symmetry) overlap strongly with the E_2 π-orbitals of the P_5 ring, placing these orbitals deeper in the bonding manifold. A similar pattern is observed for combinations of the metal d_{xz} and d_{yz} orbitals, where out-of-phase and in-phase combinations mix with p orbitals and s orbitals of the P_5 ring, respectively, with the former comprising the RAS1 space and the latter the RAS3 space. The population of the correlating antibonding orbitals in all four cases is no less than 0.06 at all temperatures, which is indicative of strong electronic correlation associated with these orbitals.

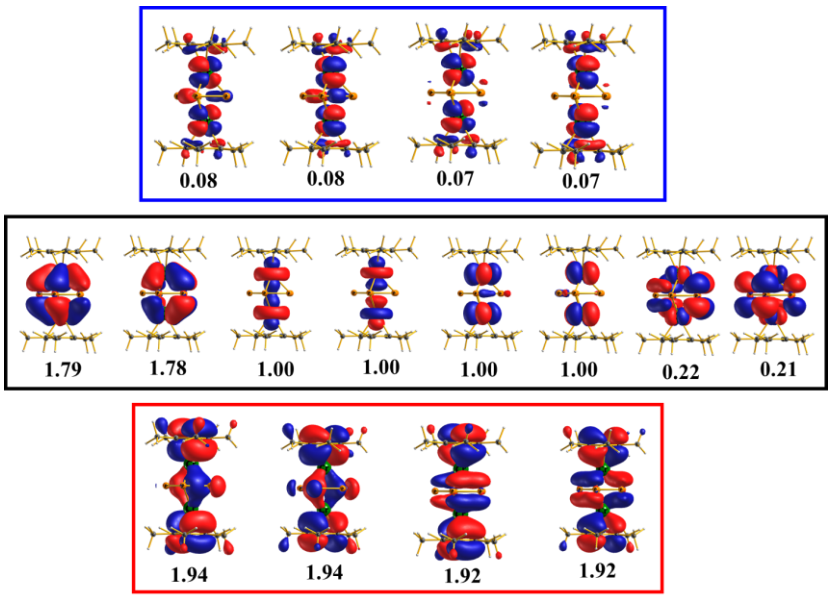

Figure **3**: Natural orbitals and occupancies for the quintet spin state from RASSCF calculations performed at the X_{290} geometry. The red box contains four RAS1 orbitals, the black box has eight RAS2 orbitals and the blue box has four RAS3 orbitals.

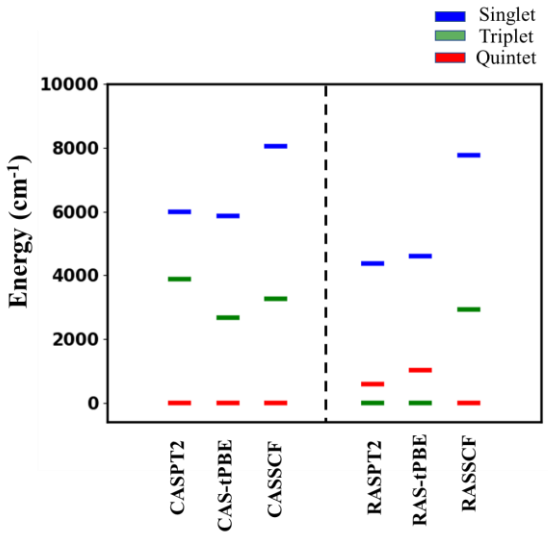

Figure **4**: Spin-state energy ladder predicted by RASSCF, RAS-tPBE, and RASPT2 methods of the dimer in the X_{110-I} geometry. The CASSCF calculations were carried out with (8e, 8o) active space and RASSCF with (16e, 16o) active space.

The critical importance of accounting for the static electron correlation associated with the RAS1/RAS3 orbital spaces manifests in the predicted spin-state energy ladders, shown for the X_{110-I} geometry in Figure **4**. The PT2 and PDFT calculations that are based on the CAS(8e,8o) reference, i.e., which omit orbitals including the chromium d_{zx} and d_{yz} combinations, disagree qualitatively with those based on the RAS(16e,16o) reference. The CAS(8e,8o)-based calculations predict a quintet ground state with the triplet being 3000 cm^{-1} or more higher in energy, depending on the dynamical correlation method. The RAS(16e,16o)-based calculations, by contrast, predict a *triplet* ground state, with the quintet state being 600 cm^{-1} or more higher in energy, depending on the dynamical correlation method. (Interestingly, the RASSCF(16e,16o) spin-state energies themselves agree qualitatively with those computed at the CASSCF(8e,8o) level, suggesting that there is a complicated interplay of static and dynamical correlation effects influencing the spin-state energy ladder.) Considering all geometries at all temperatures, RASPT2 and RAS-tPBE agree on the energy ordering of the three spin states in every case (see Table **S5** in the SI).

As noted above, between 150 K and 25 K, the magnetic susceptibility decreases rapidly, indicating changes in the spin states of the dimeric Cr(II) species. There is also a corresponding appearance in the XRD experiments of two distinct Cr(II)-dimeric units, cations I and II, with the former exhibiting an increasingly short Cr–Cr internuclear distance as the temperature is lowered, while the latter Cr–Cr distance remains reasonably constant (although at 12 K, *both* cation geometries have short Cr–Cr distances of ~2.8 Å). The temperature-dependent spin-state energy ladders of cations I and II at the RAS-tPBE level are summarized in Figure **5**.

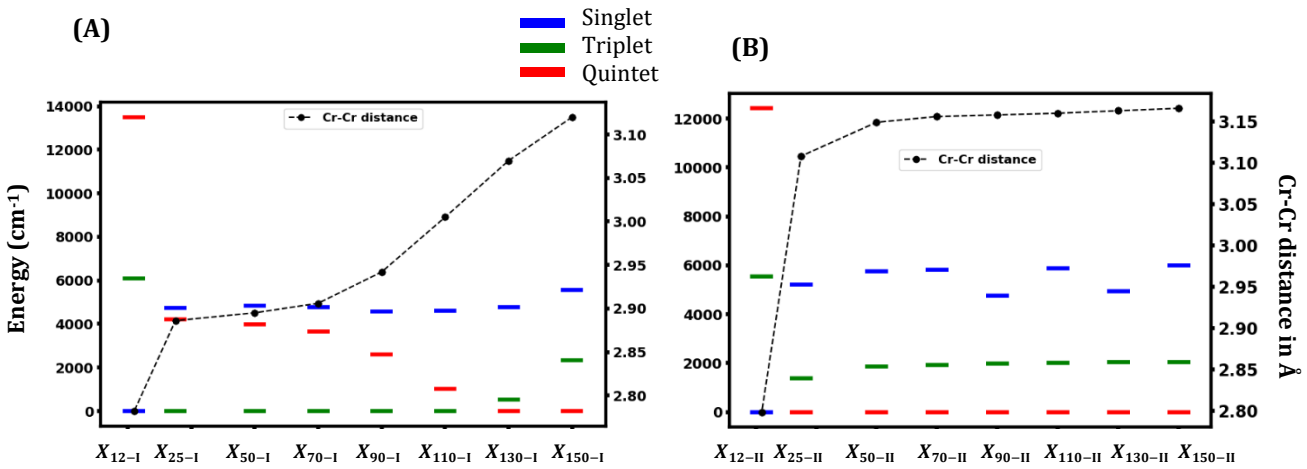

Figure **5**: Temperature variation of the spin state energies from 150K to 12K for cation I (A) and for cation II (B) obtained from RAS-tPBE calculation using (16e, 16o) active space.

As temperature decreases, and the Cr–Cr distance shrinks, the triplet state of cation I becomes increasingly stable relative to the quintet state. Between X_{130-I} and X_{110-I}, the triplet crosses the quintet to become the ground state for cation I. The singlet state energy remains roughly constant relative to the ground spin state down to X_{25-I} and then at X_{12-I}, the singlet becomes the ground state as the Cr–Cr internuclear distance for cation I drops from approximately 2.9 Å to 2.8 Å. Over that last change in temperature, the triplet and quintet spin states are each destabilized by about 10,000 cm^{-1} relative to the singlet. Cation II exhibits a simpler temperature-dependent spin-state energy ladder as its relatively constant Cr–Cr internuclear distance (down to 50 K) favors the quintet state with a quintet-triplet gap of about 2000 cm^{-1} at all temperatures (see Figure **5B**). At X_{25-II}, as the Cr–Cr distance in cation II begins to shrink, the quintet-triplet gap falls below 1400 cm^{-1}, and at X_{12-II}, the structure of cation II becomes similar to cation I and exhibits a singlet ground state.

3.2 *Interpretation of the χT vs T curve above 150K*

A key difference between our calculations and the prior literature is the spin state at high temperatures, >150 K. Only one set of magnetic data has been acquired on this system with an observed χT = 2 at 300 K which was assigned as arising from two non-interacting S = 1 Cr centers.[25,26] Our results instead suggest a well-isolated S = 2 ground state for the dimer with strongly interacting Cr centers at high temperatures. We note that strong Cr–Cr interactions are predicted with all computational methods, and across all temperatures in our study (see below), and so we sought to rationalize this difference between theory and experiment.

We propose that this discrepancy likely arises from different crystallographic domains or polymorphs in the magnetic data which is necessarily on a bulk polycrystalline sample.[55] The variable temperature crystallographic data on this compound demonstrates that at least two closely related crystallographic polymorphs are accessible which permit different Cr–Cr distances. Therefore, the presence of different crystallites/polymorphs in a bulk sample for variable temperature magnetic susceptibility could feasibly give rise to a mixture of S = 1 and S = 2 species. Our theoretical results demonstrate that some of these molecules should stay in an S = 2 state upon cooling, while others can undergo spin-crossover to an S = 1 state, consistent with the observed magnetic behavior. However, our calculations do not consider the bulk composition of different polymorphs or crystallites. Therefore, it is not surprising that our theoretical calculations on isolated dimers, which unambiguously predict an S = 2 ground state for T > 150 K (and therefore an ideal asymptotic magnetic susceptibility of $\chi T \approx 3$ cm^3 K mol^{-1}), imperfectly model the experimental data at high temperatures (see Figure **2**).

3.3 *Interpretation of the χT vs T curve below 150K*

Using these results, we can interpret the magnetic susceptibility measurements between 150K and 25 K, spanning the range between $\chi T \approx 2$ and $\chi T \approx 1$ cm^3 K mol^{-1}, respectively (Figure **2**). Initially, we note that while the Curie law predicts an asymptotic magnetic susceptibility of $\chi T \approx 3$, 1, and 0 cm^3 K mol^{-1}, for molecules in the ideal quintet, triplet, and singlet states, respectively, the experimental curve reflects the averaged contributions of all molecules/crystallites. Particularly, between cation I and cation II, the former exhibits variations in spin-state energies over the chosen temperature window while the latter maintains a stable S = 2 spin quantum number.

Importantly, this proposed model (spin transitions from S = 2 to S = 1, and finally to S = 0) provides a more reasonable interpretation of the observed structural changes in this series. Namely, if the changes in the magnetic moment between 150K and 25 K corresponded to converting one of the dimers from S = 1 to S = 0, then that dimer should not undergo additional changes between 25 and 12 K. However,

and as noted above, a significant desymmetrization of the dimer is noted upon cooling to 12 K. This further geometric change wouldn't be expected if the dimer was in an S = 0 state through this transition but is consistent with a spin-crossover event for the conversion of an S = 1 dimer to a singlet. Thus, the spin-state changes proposed here from theory provide an alternative and plausible interpretation of the magnetic and structural data in this compound.

3.4 *Roll of spin-orbit coupling at low temperatures*

Finally, we note that spin-orbit coupling modulates the magnetic moment at low temperatures. To probe this possibility, we performed zero-field splitting (ZFS) calculations including spin-orbit interactions using both multi-reference (for local ZFS) and coupled-perturbed DFT methods, which are presented in Section **S3** (and Table **S6**) of the SI. Our results suggest that the effects of zero-field splitting may become increasingly important at low-temperature regions, especially for T < 50 K. Therefore, the χT at lower temperatures 25K < T < 90K (just before the S=0 starts becoming the ground state) will be affected due to the g and D parameters and hence can deviate significantly from the perfect S =1 magnetic moment.

3.5. *Two-step spin-crossover mechanism in terms of magnetic orbitals*

Our calculations allow us to interpret the spin-crossover phenomena in this dimer more concretely. Firstly, we propose that the magnetic moment at high temperature arises from a mixture of S = 2 and S = 1 dimers in different polymorphs or crystallites. More specifically, the magnetic moment arises from the four singly occupied orbitals arising from the d_{z^2}, d_{xy}, and $d_{x^2-y^2}$ Cr orbitals (See Figure **6**). We note that for the geometry of the S = 2 dimer at 290 K, it is not possible to localize these four singly occupied orbitals into two pairs centered on the two chromium nuclei, because the d_{xy} and $d_{x^2-y^2}$ orbitals are both *symmetric* linear combinations of the chromium d orbitals.

Figure **6** displays these magnetic centers in terms of selected natural orbitals and occupancies for the quintet, triplet, and singlet electronic states at three representative geometries for which those spin states are the ground electronic states according to our RAS-tPBE calculations. At high temperatures the magnetism arises due to the symmetric and antisymmetric linear combinations of the singly occupied d_{z^2} orbitals from one magnetic unit with zero orbital angular momentum about the Cr–Cr axis (L = 0) and the other magnetic unit is the orbital pair of d_{xy} and $d_{x^2-y^2}$ orbitals, labeled in Figure **6** as the L = 2 pair. As the temperature is reduced, the P_5 ring of cation I expands, and the two Cr nuclei are brought closer together. Starting at around T = 150 K, this promotes the singlet-pairing of the two electrons in the L = 0 orbital pair, which gradually form a weak Cr–Cr covalent σ bonding interaction with a direct overlap of the d_{z^2} orbitals. This reduces the spin angular momentum of the predicted ground electronic state, from quintet to triplet. At 12 K (or < 25K), the incongruent symmetries of the L = 2 d orbitals and the pentagonal P_5 unit preferentially stabilize one orbital pair (L = 2 pair) over the other, promoting another singlet pairing and finally reducing the total spin

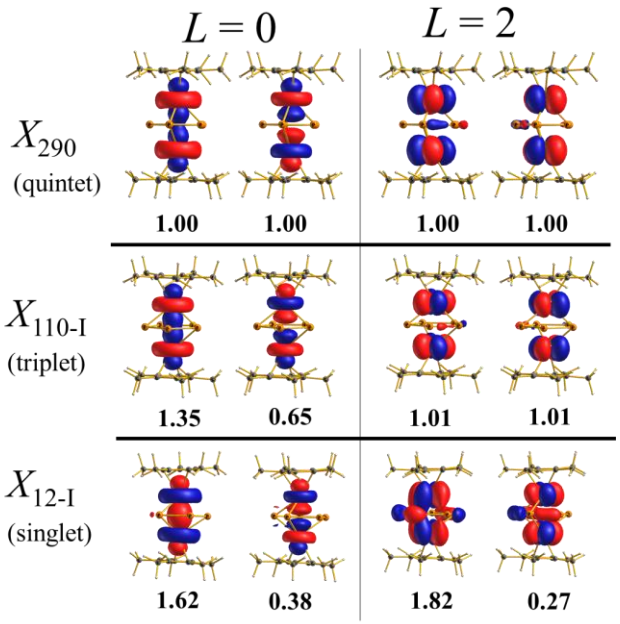

Figure **6**: Selected natural orbitals and occupancies from RASSCF (16e,16o) calculations of the ground electronic state of the dimer at three experimentally obtained geometries, ordered by apparent magnitude of angular momentum about the Cr-Cr internuclear axis and then by natural-orbital occupancies.

angular momentum of the ground electronic state to zero. This is supported by the fact that, the symmetry breaking of the P_5 unit (P-P bond length becomes dissimilar at 12 K) brings the two Cr atoms closer to the phosphorus atoms, specifically toward two of the phosphorus atoms in X_{12-I} and X_{12-II} structures.[26]

The two spin-crossover steps for cation I, here at $T \approx$ 110 K and T < 25 K differ in character. The higher-temperature step, in which the electrons in the L = 0 pair transition between spin triplet and spin singlet, can be interpreted as an antiferromagnetic interaction between two Cr atoms: structural changes in the ligand promote the formation of a d_{z^2}–d_{z^2} covalent bond. The lower-temperature crossover, on the other hand, should be understood primarily in terms of a strong ligand-field effect splitting otherwise degenerate L = 2, d orbitals on both chromium atoms simultaneously. The effects of spin-orbit coupling likely play a significant role in the region 25K < T < 50K as the spin multiplets split due to zero-field splitting (see Table **S6**). For cation II, a direct conversion to the S = 0 state occurs below 25 K, and hence a sharp spin transition takes place at the susceptibility curve.

4. Conclusion

Using multiconfiguration pair-density functional theory we have provided for the first time a detailed picture of the spin-crossover behavior of the dimeric triple-decker Cr(II) complex.

The aromatic P_5 ring generates a strong ligand field which plays a decisive role in determining the total spin of the ground electronic state of the molecule. At all temperatures, four of the eight formally unpaired *d* electrons of the Cr(II) ions are involved in $p\pi$-$d\pi$ bonds with the P_5 ring. In the spin-crossover temperature range (12 K < T < 150 K), our multireference calculations show two different spin-crossover behaviors for the two dimeric units observed in XRD experiments by Goeta, A. *et al*.[26] For the unit labeled "cation I," our calculations show a two-step crossover from quintet to triplet and then to singlet corresponding to the gradually-decreasing Cr–Cr internuclear distance; for the unit labeled "cation II", our calculations show an abrupt single-step crossover at T < 25 K from quintet to singlet. These results provide a detailed understanding of Goeta *et al*.'s analysis[26] of the observed magnetic susceptibility (Figure **2**).

Natural-orbital analysis of our RASSCF(16e,16o) calculations suggests that the two component S = 1 units of this system are best understood not as two S = 1 chromium ions, but as two pairs of electrons occupying two pairs of orbitals distinguished by the magnitude of their angular momentum about the Cr–Cr internuclear axis. The two-step crossover of cation I consists of the reduction from S = 2 to S = 0 of these two electron pairs at two different temperatures. Our analysis supports some aspects of both of the two proposed spin-crossover mechanisms of Goeta, A. *et al*.:

1. The model of antiferromagnetic interactions between chromium atoms is consistent with our picture of the transition of cation I from quintet to triplet ground state at about T = 110 K: our natural orbitals show the formation of a direct d_{z^2}-d_{z^2} bonding interaction at this temperature and below.

2. The model of the ligand field preferentially stabilizing the low-spin state of the metal ions at lower temperatures is consistent with our picture of the transition of cation I to the singlet ground state at T < 25 K, in which one of the L = 2 *d*-orbital pair is preferentially stabilized simultaneously on both Cr atoms.

We note that both of the spin-crossover steps involve natural orbital occupancies in the lower-spin states that deviate strongly from unity, implying that the Heisenberg–Dirac–van Vleck Hamiltonian[56,57,58] and the Landé[59] formula for spin-state energies of polymetallic magnetic molecules do not apply and should not be used (at least as models of these particular spin-crossover transitions) regardless of whether one considers the two magnetic centers to be the two chromium atoms or the two orbital pairs.

In future investigations of the spin-crossover mechanism of this and similar molecules, it will be important to consider the effects of thermal vibrations at higher temperatures. Furthermore, our results here motivate a deeper investigation of the presence of multiple polymorphs in polycrystalline samples of this Cr dimer, particularly in explaining the bulk magnetic moment at room temperature.

On the other hand, spin-orbit coupling is expected to play a significant role in the low-temperature transition, particularly around T < 50 K. Our NEVPT2-SO calculations suggest significant zero-field splitting (local) for X_{30-I} and that the effect of spin-orbit coupling on the spin-crossover mechanism should be considered more closely in future studies.

Finally, the agreement between RAS-tPBE and RASPT2 results is encouraging, as the former is significantly less computationally costly than the latter. We envision using the proposed affordable methodology to explore and predict SCO in other multimetallic complexes.

ASSOCIATED CONTENT

The supporting information contains results of preliminary calculations additional numerical data, optimized geometries, orbitals, results for preliminary magnetic anisotropy calculations accounting for the effects of spin-orbit coupling, and tables for the absolute total energies.

AUTHOR INFORMATION

Corresponding Author

* **Laura Gagliardi**

Department of Chemistry, Pritzker School of Molecular Engineering, James Franck Institute,Director of the Chicago Center for Theoretical Chemistry, The University of Chicago, Chicago, IL-60637 USA

Email: lgagliardi@uchicago.edu

Author Contributions

The manuscript was written through contributions of all authors. / All authors have given approval to the final version of the manuscript.

ACKNOWLEDGMENT

This work was partially supported by the Air Force Office of Scientific Research (Grant No. *FA9550-16-1-0134)*. JSA gratefully acknowledges support from the Dreyfus Foundation for a teacher-scholar award (TC-21-064). The authors gratefully acknowledge the University of Chicago Research Computing Center (RCC) for the computational resources.

REFERENCES

(1) Gütlich, P.; Goodwin, H. A. Spin Crossover—An Overall Perspective. **2012**, *1*, 1–47. https://doi.org/10.1007/b13527.

(2) Kahn, O.; Martinez, C. J. Spin-Transition Polymers: From Molecular Materials toward Memory Devices. *Science (80-.).* **1998**, *279* (5347), 44–48. https://doi.org/10.1126/science.279.5347.44.

(3) Real, J. A.; Bolvin, H.; Bousseksou, A.; Dworkin, A.; Kahn, O.; Varret, F.; Zarembowitch, J. Two-Step Spin Crossover in the New Dinuclear Compound [Fe(Bt)(NCS)2]2bpym, with Bt =

2,2′-Bi-2-Thiazoline and Bpym = 2,2′-Bipyrimidine: Experimental Investigation and Theoretical Approach. *J. Am. Chem. Soc.* **1992**, *114* (12), 4650–4658. https://doi.org/10.1021/ja00038a031.

(4) Gütlich, P.; Garcia, Y.; Goodwin, H. A. Spin Crossover Phenomena in Fe(II) Complexes. *Chem. Soc. Rev.* **2000**, *29* (6), 419–427. https://doi.org/10.1039/b003504l.

(5) Halcrow, M. A. *Spin-Crossover Materials: Properties and Applications*; John Wiley & Sons, 2013.

(6) Cointe, M. B.; Lescoue, R. On/O Ff Photoswitching in a Cyanide-Bridged {Fe 2 Co 2 } Magnetic Molecular Square. **2012**, 10–13.

(7) Mondal, A.; Li, Y.; Chamoreau, L. M.; Seuleiman, M.; Rechignat, L.; Bousseksou, A.; Boillot, M. L.; Lescouëzec, R. Photo- and Thermo-Induced Spin Crossover in a Cyanide-Bridged (MoV2FeII2) Rhombus Molecule. *Chem. Commun.* **2014**, *50* (22), 2893–2895. https://doi.org/10.1039/c3cc49164a.

(8) Stauch, T.; Chakraborty, R.; Head-Gordon, M. Quantum Chemical Modeling of Pressure-Induced Spin Crossover in Octahedral Metal-Ligand Complexes. *ChemPhysChem* **2019**, *20* (21), 2742–2747. https://doi.org/10.1002/cphc.201900853.

(9) Shepherd, H. J.; Rosa, P.; Vendier, L.; Casati, N.; Létard, J. F.; Bousseksou, A.; Guionneau, P.; Molnár, G. High-Pressure Spin-Crossover in a Dinuclear Fe(Ii) Complex. *Phys. Chem. Chem. Phys.* **2012**, *14* (15), 5265–5271. https://doi.org/10.1039/c2cp23940j.

(10) Coronado, E.; Day, P. Magnetic Molecular Conductors. *Chem. Rev.* **2004**, *104* (11), 5419–5448. https://doi.org/10.1021/cr030641n.

(11) Senthil Kumar, K.; Ruben, M. Emerging Trends in Spin Crossover (SCO) Based Functional Materials and Devices. *Coord. Chem. Rev.* **2017**, *346*, 176–205. https://doi.org/10.1016/j.ccr.2017.03.024.

(12) Gütlich, P.; Garcia, Y.; Woike, T. *Photoswitchable Coordination Compounds*; 2001; Vol. 219–221. https://doi.org/10.1016/S0010-8545(01)00381-2.

(13) Molnár, G.; Mikolasek, M.; Ridier, K.; Fahs, A.; Nicolazzi, W.; Bousseksou, A. Molecular Spin Crossover Materials: Review of the Lattice Dynamical Properties. *Ann. Phys.* **2019**, *531* (10), 1–21. https://doi.org/10.1002/andp.201900076.

(14) Oppermann, M.; Zinna, F.; Lacour, J.; Chergui, M. Chiral Control of Spin-Crossover Dynamics in Fe(II) Complexes. *Nat. Chem.* **2022**, *14* (July). https://doi.org/10.1038/s41557-022-00933-0.

(15) Goodwin, H. A. Spin Transitions in Six-Coordinate Iron(II) Complexes. *Coord. Chem. Rev.* **1976**, *18* (3), 293–325. https://doi.org/10.1016/S0010-8545(00)80430-0.

(16) Mondal, D. J.; Mondal, A.; Paul, A.; Konar, S. Guest-Induced Multistep-to-One-Step Reversible Spin Transition with Enhanced Hysteresis in a 2D Hofmann Framework. *Inorg. Chem.* **2022**, *61* (11), 4572–4580. https://doi.org/10.1021/acs.inorgchem.1c03306.

(17) Shatruk, M.; Phan, H.; Chrisostomo, B. A.; Suleimenova, A. Symmetry-Breaking Structural Phase Transitions in Spin Crossover Complexes. *Coord. Chem. Rev.* **2015**, *289–290* (1), 62–73. https://doi.org/10.1016/j.ccr.2014.09.018.

(18) Sim, P. G.; Sinn, E. First Manganese(III) Spin Crossover, First D4 Crossover. Comment on Cytochrome Oxidase. *J. Am. Chem. Soc.* **1981**, *103* (1), 241–243. https://doi.org/10.1021/ja00391a067.

(19) Halepoto, D. M.; Holt, D. G. L.; Larkworthy, L. F.; Leigh, G. J.; Povey, D. C.; Smith, G. W. Spin Crossover in Chromium(II) Complexes and the Crystal and Molecular Structure of the High Spin Form of Bis[1,2-Bis(Diethylphosphino)Ethane]Di-Iodochromium(II). *J. Chem. Soc. Chem. Commun.* **1989**, No. 18, 1322–1323. https://doi.org/10.1039/C39890001322.

(20) Tissot, A.; Bertoni, R.; Collet, E.; Toupet, L.; Boillot, M. L. The Cooperative Spin-State Transition of an Iron(Iii) Compound [Fe III(3-MeO-SalEen)2]PF6: Thermal- vs. Ultra-Fast Photo-Switching. *J. Mater. Chem.* **2011**, *21* (45), 18347–18353. https://doi.org/10.1039/c1jm14163e.

(21) Ghosh, S.; Ghosh, S.; Kamilya, S.; Mandal, S.; Mehta, S.; Mondal, A. Impact of Counteranion on Reversible Spin-State Switching in a Series of Cobalt(II) Complexes Containing a Redox-Active Ethylenedioxythiophene-Based Terpyridine Ligand. *Inorg. Chem.* **2022**, *61* (43), 17080–17088. https://doi.org/10.1021/acs.inorgchem.2c02313.

(22) Pantazis, D. A. Meeting the Challenge of Magnetic Coupling in a Triply-Bridged Chromium Dimer: Complementary Broken-Symmetry Density Functional Theory and Multireference Density Matrix Renormalization Group Perspectives. *J. Chem. Theory Comput.* **2019**, *15* (2), 938–948. https://doi.org/10.1021/acs.jctc.8b00969.

(23) Sharma, P.; Truhlar, D. G.; Gagliardi, L. Magnetic Coupling in a Tris-Hydroxo-Bridged Chromium Dimer Occurs through Ligand Mediated Superexchange in Conjunction with Through-Space Coupling. *J. Am. Chem. Soc.* **2020**, *142* (39), 16644–16650. https://doi.org/10.1021/jacs.0c06399.

(24) Pandharkar, R.; Hermes, M. R.; Cramer, C. J.; Gagliardi, L. Spin-State Ordering in Metal-Based Compounds Using the Localized Active Space Self-Consistent Field Method. *J. Phys. Chem. Lett.* **2019**, *10* (18), 5507–5513. https://doi.org/10.1021/acs.jpclett.9b02077.

(25) Hughes, A. K.; Murphy, V. J.; O'Hare, D. Synthesis, X-Ray Structure and Spin Crossover in the Triple-Decker Complex [(H5-C5Me5)Cr(M2: H5-P5)Cr(H5-C5Me 5)]+[A]- (A=PF6, SbF6). *J. Chem. Soc. Chem. Commun.* **1994**, *409* (2), 163–164. https://doi.org/10.1039/C39940000163.

(26) Goeta, A. E.; Howard, J. A. K.; Hughes, A. K.; O'Hare, D.; Copley, R. C. B. Structural-Magnetic Correlations on the First Dinuclear Spin Crossover D4 System. *J. Mater. Chem.* **2007**, *17* (5), 485–492. https://doi.org/10.1039/b612121g.

(27) Cirera, J.; Via-Nadal, M.; Ruiz, E. Benchmarking Density Functional Methods for Calculation of State Energies of First Row Spin-Crossover Molecules. *Inorg. Chem.* **2018**, *57* (22), 14097–14105. https://doi.org/10.1021/acs.inorgchem.8b01821.

(28) Ye, S.; Neese, F. Accurate Modeling of Spin-State Energetics in Spin-Crossover Systems with Modern Density Functional Theory. *Inorg. Chem.* **2010**, *49* (3), 772–774. https://doi.org/10.1021/ic902365a.

(29) De, S.; Chamoreau, L. M.; Said, H. El; Li, Y.; Flambard, A.; Boillot, M. L.; Tewary, S.; Rajaraman, G.; Lescouëzec, R. Thermally-Induced Spin Crossover and LIESST Effect in the Neutral [FeII(Mebik)2(NCX)2] Complexes: Variable-Temperature Structural, Magnetic, and Optical Studies (X = S, Se; Mebik = Bis(1-Methylimidazol-2-Yl)Ketone). *Front. Chem.* **2018**, *6* (AUG), 1–15. https://doi.org/10.3389/fchem.2018.00326.

(30) De, S.; Tewary, S.; Garnier, D.; Li, Y.; Gontard, G.; Lisnard, L.;

Flambard, A.; Breher, F.; Boillot, M. L.; Rajaraman, G.; Lescouëzec, R. Solution and Solid-State Study of the Spin-Crossover [FeII(R-Bik)3](BF4)2 Complexes (R = Me, Et, Vinyl). *Eur. J. Inorg. Chem.* **2018**, *2018* (3), 414–428. https://doi.org/10.1002/ejic.201701013.

(31) Cramer, C. J.; Truhlar, D. G. Density Functional Theory for Transition Metals and Transition Metal Chemistry. *Phys. Chem. Chem. Phys.* **2009**, *11* (46), 10757–10816. https://doi.org/10.1039/b907148b.

(32) Flöser, B. M.; Guo, Y.; Riplinger, C.; Tuczek, F.; Neese, F. Detailed Pair Natural Orbital-Based Coupled Cluster Studies of Spin Crossover Energetics. *J. Chem. Theory Comput.* **2020**, *16* (4), 2224–2235. https://doi.org/10.1021/acs.jctc.9b01109.

(33) Drosou, M.; Mitsopoulou, C. A.; Pantazis, D. A. Reconciling Local Coupled Cluster with Multireference Approaches for Transition Metal Spin-State Energetics. *J. Chem. Theory Comput.* **2022**. https://doi.org/10.1021/acs.jctc.2c00265.

(34) Vela, S.; Fumanal, M.; Ribas-Ariño, J.; Robert, V. On the Zeroth-Order Hamiltonian for CASPT2 Calculations of Spin Crossover Compounds. *J. Comput. Chem.* **2016**, *37* (10), 947–953. https://doi.org/10.1002/jcc.24283.

(35) Finney, B. A.; Chowdhury, S. R.; Kirkvold, C.; Vlaisavljevich, B. CASPT2 Molecular Geometries of Fe(Ii) Spin-Crossover Complexes. *Phys. Chem. Chem. Phys.* **2022**, *24* (3), 1390–1398. https://doi.org/10.1039/d1cp04885f.

(36) Phung, Q. M.; Domingo, A.; Pierloot, K. Dinuclear Iron(II) Spin-Crossover Compounds: A Theoretical Study. *Chem. - A Eur. J.* **2018**, *24* (20), 5183–5190. https://doi.org/10.1002/chem.201704441.

(37) Larsson, H. R.; Zhai, H.; Umrigar, C. J.; Chan, G. K.-L. The Chromium Dimer: Closing a Chapter of Quantum Chemistry. *J. Am. Chem. Soc.* **2022**. https://doi.org/10.1021/jacs.2c06357.

(38) Rani, D. U.; Prasad, D. L. V. K.; Nixon, J. F.; Jemmis, E. D. Electronic Structure and Bonding Studies on Triple-Decker Sandwich Complexes with a P6 Middle Ring. *J. Comput. Chem.* **2007**, *28* (1), 310–319. https://doi.org/https://doi.org/10.1002/jcc.20521.

(39) Mondal, S.; Chen, W.-X.; Sun, Z.-M.; McGrady, J. E. Synthesis, Structure and Bonding in Pentagonal Bipyramidal Cluster Compounds Containing a Cyclo-Sn5 Ring, [(CO)3MSn5M(CO)3]4− (M = Cr, Mo). *Inorganics* **2022**, *10* (6), 75. https://doi.org/10.3390/inorganics10060075.

(40) Gardner, B. M.; Tuna, F.; McInnes, E. J. L.; McMaster, J.; Lewis, W.; Blake, A. J.; Liddle, S. T. An Inverted-Sandwich Diuranium μ-H5:H5-Cyclo-P5 Complex Supported by U-P5 δ-Bonding. *Angew. Chemie - Int. Ed.* **2015**, *54* (24), 7068–7072. https://doi.org/10.1002/anie.201501728.

(41) Wang, Z. C.; Qiao, L.; Sun, Z. M.; Scheer, M. Inorganic Ferrocene Analogue [Fe(P4)2]2-. *J. Am. Chem. Soc.* **2022**, *144* (15), 6698–6702. https://doi.org/10.1021/jacs.2c01750.

(42) Olsen, J.; Roos, B. O.; Jørgensen, P.; Jensen, H. J. A. Determinant Based Configuration Interaction Algorithms for Complete and Restricted Configuration Interaction Spaces. *J. Chem. Phys.* **1988**, *89* (4), 2185–2192. https://doi.org/10.1063/1.455063.

(43) Malmqvist, P. Å.; Rendell, A.; Roos, B. O. The Restricted Active Space Self-Consistent-Field Method, Implemented with a Split Graph Unitary Group Approach. *J. Phys. Chem.* **1990**, *94* (14), 5477–5482. https://doi.org/10.1021/j100377a011.

(44) Li Manni, G.; Carlson, R. K.; Luo, S.; Ma, D.; Olsen, J.; Truhlar, D. G.; Gagliardi, L. Multiconfiguration Pair-Density Functional Theory. *J. Chem. Theory Comput.* **2014**, *10* (9), 3669–3680. https://doi.org/10.1021/ct500483t.

(45) Gagliardi, L.; Truhlar, D. G.; Manni, G. L.; Carlson, R. K.; Hoyer, C. E.; Bao, J. L. Multiconfiguration Pair-Density Functional Theory: A New Way to Treat Strongly Correlated Systems. *Acc. Chem. Res.* **2017**, *50* (1), 66–73. https://doi.org/10.1021/acs.accounts.6b00471.

(46) Wilbraham, L.; Verma, P.; Truhlar, D. G.; Gagliardi, L.; Ciofini, I. Multiconfiguration Pair-Density Functional Theory Predicts Spin-State Ordering in Iron Complexes with the Same Accuracy as Complete Active Space Second-Order Perturbation Theory at a Significantly Reduced Computational Cost. *J. Phys. Chem. Lett.* **2017**, *8* (9), 2026–2030. https://doi.org/10.1021/acs.jpclett.7b00570.

(47) Pandharkar, R.; Hermes, M. R.; Cramer, C. J.; Truhlar, D. G.; Gagliardi, L. Localized Active Space Pair-Density Functional Theory. *J. Chem. Theory Comput.* **2021**, *17* (5), 2843–2851. https://doi.org/10.1021/acs.jctc.1c00067.

(48) Stroscio, G. D.; Zhou, C.; Truhlar, D. G.; Gagliardi, L. Multiconfiguration Pair-Density Functional Theory Calculations of Iron(II) Porphyrin: Effects of Hybrid Pair-Density Functionals and Expanded RAS and DMRG Active Spaces on Spin-State Orderings. *J. Phys. Chem. A* **2022**, *126* (24), 3957–3963. https://doi.org/10.1021/acs.jpca.2c02347.

(49) Zhou, C.; Hermes, M. R.; Wu, D.; Bao, J. J.; Pandharkar, R.; King, D. S.; Zhang, D.; Scott, T. R.; Lykhin, A. O.; Gagliardi, L.; Truhlar, D. G. Electronic Structure of Strongly Correlated Systems: Recent Developments in Multiconfiguration Pair-Density Functional Theory and Multiconfiguration Nonclassical-Energy Functional Theory. *Chem. Sci.* **2022**, 7685–7706. https://doi.org/10.1039/d2sc01022d.

(50) Sauza-De La Vega, A.; Pandharkar, R.; Stroscio, G. D.; Sarkar, A.; Truhlar, D. G.; Gagliardi, L. Multiconfiguration Pair-Density Functional Theory for Chromium(IV) Molecular Qubits. *J. Am. Chem. Soc.* **2022**, No. Iv. https://doi.org/10.1021/jacsau.2c00306.

(51) Ghigo, G.; Roos, B. O.; Malmqvist, P. Å. A Modified Definition of the Zeroth-Order Hamiltonian in Multiconfigurational Perturbation Theory (CASPT2). *Chem. Phys. Lett.* **2004**, *396* (1–3), 142–149. https://doi.org/10.1016/j.cplett.2004.08.032.

(52) Aquilante, F.; Lindh, R.; Bondo Pedersen, T. Unbiased Auxiliary Basis Sets for Accurate Two-Electron Integral Approximations. *J. Chem. Phys.* **2007**, *127* (11). https://doi.org/10.1063/1.2777146.

(53) Neese, F. Software Update: The ORCA Program System, Version 4.0. *Wiley Interdiscip. Rev. Comput. Mol. Sci.* **2018**, *8* (1), 4–9. https://doi.org/10.1002/wcms.1327.

(54) Fdez. Galván, I.; Vacher, M.; Alavi, A.; Angeli, C.; Aquilante, F.; Autschbach, J.; Bao, J. J.; Bokarev, S. I.; Bogdanov, N. A.; Carlson, R. K.; Chibotaru, L. F.; Creutzberg, J.; Dattani, N.; Delcey, M. G.; Dong, S. S.; Dreuw, A.; Freitag, L.; Frutos, L. M.; Gagliardi, L.; Gendron, F.; Giussani, A.; González, L.; Grell, G.; Guo, M.; Hoyer, C. E.; Johansson, M.; Keller, S.; Knecht, S.; Kovačević, G.; Källman, E.; Li Manni, G.; Lundberg, M.; Ma, Y.; Mai, S.; Malhado, J. P.; Malmqvist, P. Å.; Marquetand, P.; Mewes, S. A.; Norell, J.; Olivucci, M.; Oppel, M.; Phung, Q. M.; Pierloot, K.; Plasser, F.; Reiher, M.; Sand, A. M.; Schapiro, I.; Sharma, P.; Stein, C. J.; Sørensen, L. K.; Truhlar, D. G.; Ugandi, M.; Ungur, L.; Valentini, A.; Vancoillie, S.; Veryazov, V.; Weser, O.; Wesołowski, T. A.; Widmark, P. O.; Wouters, S.; Zech, A.;

Zobel, J. P.; Lindh, R. OpenMolcas: From Source Code to Insight. *J. Chem. Theory Comput.* **2019**, *15* (11), 5925–5964. https://doi.org/10.1021/acs.jctc.9b00532.

(55) Tao, J.; Wei, R. J.; Huang, R. Bin; Zheng, L. S. Polymorphism in Spin-Crossover Systems. *Chem. Soc. Rev.* **2012**, *41* (2), 703–737. https://doi.org/10.1039/c1cs15136c.

(56) Heisenberg, W. Zur Theorie Des Ferromagnetismus. *Zeitschrift für Phys.* **1928**, *49* (9–10), 619–636. https://doi.org/10.1007/BF01328601.

(57) Downloaded from Https://Royalsocietypublishing.Org/ on 18 January 2023 P . A . M . Dirac . Downloaded from Https://Royalsocietypublishing.Org/ on 18 January 2023. **1926**, *33* (1).

(58) Van Vleck, J. H. A Survey of the Theory of Ferromagnetism. *Rev. Mod. Phys.* **1945**, *17* (1), 27–47. https://doi.org/10.1103/RevModPhys.17.27.

(59) Landé, A. Termstruktur Und Zeemaneffekt Der Multipletts. *Zeitschrift für Phys.* **1923**, *19* (1), 112–123. https://doi.org/10.1007/BF01327550.

TOC:

Anti-ferromagnetic and ligand field interactions in a triple-decker Cr-dimer.